Rough surface RCS measurements and simulations using the Physical Optics Approximation

Charlotte Corbel, Christophe Bourlier, Nicolas Pinel, Janic Chauveau

Rough surface RCS measurements and simulations using the Physical Optics Approximation

Charlotte Corbel, Christophe Bourlier, Nicolas Pinel, and Janic Chauveau

Abstract—**The objective of this article is to develop innovative approaches to obtain analytical expressions of the Radar Cross Section (RCS) of perfectly-conducting random rough surfaces under the Physical Optics (PO) approximation. The led approaches take into account the specific geometrical properties of the considered surfaces to calculate their RCS. The objective is to reduce the computing time with respect to the numerical PO technique, which requires two numerical integrations. All developed approaches are validated by comparison with a commercial code (the MLFMM of FEKO), used as a reference, and with measurements performed on three selected rough surfaces samples.**

Index Terms—**Physical Optics, Random rough surfaces, RCS calculation, RCS measurement, diffraction, asymptotic methods.**

I. Introduction

THE phenomenon of diffraction by random rough surfaces is of prime interest in various domains and for numerous applications such as Earth observation (both oceanic and continental surfaces remote sensing), military operations, communications, and also in optical domain for man-made surfaces like quasi-random gratings or antireflection coatings. Rigorous methods such as the Method of Moments are widely developed [1],[2] to calculate a surface Radar Cross Section (RCS). However, these rigorous numerical methods can become highly time-consuming when the surface size with respect to the wavelength increases, making the use of these methods prohibitive for real-time operational requirements. To cope with the numerical complexity of realistic scattering problems, numerous asymptotic methods have emerged, most of them being listed in [3]. Physical Optics (PO) approximation, or Kirchhoff approximation [4]-[7], is one of the widely used high-frequency asymptotic techniques to accelerate the RCS calculation, in its restricted validity domain.

The purpose of this paper is to develop new approaches to expedite the PO technique. These approaches use the specific geometrical properties of the studied random rough surfaces to calculate analytically the double integration that lies in the expression of their RCS. The preliminary step is the development of a numerical PO method, source of the other ones. Then, two different approaches are led. The first one is a global approach that consists in obtaining the random rough surface RCS by applying a correction factor to the RCS of a smooth object; the factor is calculated thanks to the statistical properties of the surface and is a function of the surface height standard deviation. The second approach relies on the decomposition of a random rough surface heights into a sum of cosine functions components and the use of the Bessel functions properties to calculate the surface RCS. The developed approaches use additional simplifications with respect to the assumptions PO relies on, thus these approaches are not expected to get a wider validity domain than PO, but a more rapid calculation.

A reference method is required to assess the validity domain of the developed approaches. The MLFMM (Multilevel Fast Multi-Pole Method) of commercial code FEKO has been chosen as a such reference. For the calculation of rough surface RCS, showing a simple geometry, as considered in this paper, its results are satisfactory and reliable [8]. Ultimately, the methods validation is performed by comparison with experimental measurements that constitute the second main part of this study. To determine the validity domain of the new developed approaches, a panel of targets is modeled and a wide observation angles range $[-90°, +90°]$ is considered. The surface roughnesses variety is obtained by using several surface rms heights, correlation lengths, autocorrelation functions but also a large frequency range. Three rough surface samples have been defined and built; their RCS have been measured from 2 to 18 GHz in an anechoic chamber.

This paper is organized as follows: first, the random rough surfaces generation is introduced and the developed numerical PO method presented; then, the statistical approach and results are shown. The third part deals with the deterministic approach based on the surface decomposition into cosine components, and the last part is dedicated to the measurements and their comparison with simulations.

The time convention $e^{+i\omega t}$ is omitted throughout the paper.

II. Preamble: Rough surfaces and Physical Optics

A. Random rough surface generation

Using a statistical description, a rough surface defined by points of coordinates $(x, y, z(x, y))$ can be described with deterministic statistical quantities such as surface height distribution and autocorrelation function. The selected height probability density function (PDF) $p_z(z)$ is Gaussian, centered (zero mean value $\langle z \rangle = 0$) and with standard deviation

C. Bourlier, C. Corbel and N. Pinel are with IETR (Institut d'Electronique et des Télécommunications de Rennes) laboratory, LUNAM Université, Université de Nantes, La Chantrerie, 44306 Nantes, France. E-mail: charlotte.corbel@univ-nantes.fr)

J. Chauveau is with the DGA/DT/MI (Direction Générale de l'Armement – Direction Technique – Maîtrise de l'Information), CGN1 division, 35170 Bruz, France.

$\sigma_z = \sqrt{\langle z^2 \rangle} = \sqrt{\int_{-\infty}^{\infty} z^2 p_z(z) dz}$:

$$p_z(z) = \frac{1}{\sigma_z \sqrt{2\pi}} e^{-\frac{z^2}{2\sigma_z^2}}$$

and checks:

$$\langle 1 \rangle = \int_{-\infty}^{\infty} p_z(z) dz = 1, \quad \langle z \rangle = \int_{-\infty}^{\infty} z p_z(z) dz = 0$$

In the whole paper, the symbol $\langle ... \rangle$ stands for the ensemble average. The height autocorrelation function (second-order statistical moment) is the statistical average of two surface points heights product:

$$C_z(\mathbf{r}) = \langle z(\mathbf{r}_1) z^*(\mathbf{r}_1 + \mathbf{r}) \rangle = \langle z(\mathbf{r}_1) z(\mathbf{r}_1 + \mathbf{r}) \rangle \quad \text{since} \quad z \in \mathbb{R}$$

where $\mathbf{r} = (x, y)$. The surface height autocorrelation function can be of Gaussian or exponential type:

$$C_z(x,y) = \begin{cases} \sigma_z^2 e^{\left[- \left(\frac{x}{L_{cx}} \right)^2 - \left(\frac{y}{L_{cy}} \right)^2 \right]} & \text{Gaussian} \\ \sigma_z^2 e^{\left(- \frac{|x|}{L_{cx}} - \frac{|y|}{L_{cy}} \right)} & \text{exponential} \end{cases},$$

with $\{L_{cx}, L_{cy}\}$ the surface correlation length along $\hat{\mathbf{x}}$ and $\hat{\mathbf{y}}$ directions, respectively. Random surfaces generation requires to use the surface power spectral density (also called surface height spectrum), which is the Fourier transform of the autocorrelation function and is thus defined as:

$$S_z(k_x, k_y) = \frac{1}{(2\pi)^2} \int_{-\infty}^{+\infty} C_z(x,y) e^{-j(k_x x + k_y y)} dx dy$$

$$= \begin{cases} \frac{\sigma_z^2 L_{cx} L_{cy}}{4\pi} e^{\left[- \left(\frac{k_x L_{cx}}{2} \right)^2 - \left(\frac{k_y L_{cy}}{2} \right)^2 \right]} & \text{Gaussian} \\ \frac{\sigma_z^2 L_{cx} L_{cy}}{\pi^2} \frac{1}{\left[1 + (k_x L_{cx})^2\right]} \frac{1}{\left[1 + (k_y L_{cy})^2\right]} & \text{exponential} \end{cases},$$

with $\{k_x, k_y\}$ (wavenumbers) the duals of $\{x, y\}$. The surface height profile is fully determined by the height probability density $p_z(z)$ and autocorrelation $C_z(\mathbf{r})$ (or spectrum $S_z(\mathbf{k})$) functions; indeed, all statistical moments of a Gaussian distribution profile are related to the first two ones [6].

Three surfaces are selected to perform the comparison of the various developed approaches. The theoretical parameters used to generate the surfaces are summarized in Table I and their real statistical parameters, calculated from the generated surfaces, in Table II. The roughness parameters (L_c, autocorrelation function, ratio σ_z/λ with λ the wavelength) have been chosen to get a wide domain of surface roughnesses in the frequency range 2 GHz to 18 GHz, where measurements were possible. Isotropic surfaces have been generated with the same correlation length along $\hat{\mathbf{x}}$ and $\hat{\mathbf{y}}$ directions: $L_{c_x} = L_{c_y} = L_c$. Samples with the defined profiles have been built and their RCS have been measured in an anechoic chamber. A minimum acceptable sample size $L = L_x = L_y$ is required to apply PO ($L >> \lambda$) but also statistical operations ($L >> L_c$). The main limitation for the manufactured samples selection was linked to their handling and measurement possibility, hence their size has been restricted to 80 cm and their shape has been chosen circular to limit their weight to 50 kg. In the worst case, at 2 GHz, the ratio of the surface length to the wavelength λ is 5.33.

no.	Shape	Diameter	Correlation	σ_z	L_c	σ_γ
1	circle	80 cm	Gaussian	0.75 cm	5 cm	0.21
2	circle	80 cm	exponential	0.75 cm	5 cm	-
3	circle	80 cm	Gaussian	0.75 cm	3 cm	0.35

TABLE I
3 SELECTED SAMPLES THEORETICAL PARAMETERS.

no.	σ_z	σ_{γ_x}	σ_{γ_y}	$\langle \gamma_x \rangle$	$\langle \gamma_y \rangle$
1	0.7558 cm	0.1959	0.2198	0.0025	-0.0002
2	0.7488 cm	0.8074	0.7972	0.0018	0.0014
3	0.7496 cm	0.3564	0.3478	0.0018	0.0009

TABLE II
3 GENERATED SAMPLES STATISTICAL PARAMETERS.

B. The Physical Optics (PO) approximation

Assuming a perfectly conducting target, its diffraction matrix $\bar{\mathbf{S}} = \begin{bmatrix} S_{\theta\theta} & S_{\theta\phi} \\ S_{\phi\theta} & S_{\phi\phi} \end{bmatrix}$ in vacuum can be expressed, under the PO approximation, as:

$$\bar{\mathbf{S}} = P \int\int_{\Sigma_{PO}} (\bar{\mathbf{a}}_1 \gamma_x + \bar{\mathbf{a}}_2 \gamma_y + \bar{\mathbf{a}}_3) e^{i[b_1 x + b_2 y + b_3 z(x,y)]} dx dy \tag{1}$$

with $P = (-i\omega_0 \mu_0 / 2\eta_0 \pi R') e^{-ik_0 R'}$ a scalar quantity depending on the observation distance R', the frequency f_0 by way of $\omega_0 = 2\pi f_0$, and the propagation medium dielectric properties: μ_0 the permeability, η_0 the impedance and k_0 the wavenumber in vacuum. $\gamma_x = \partial z / \partial x$ is the slope along $\hat{\mathbf{x}}$ direction and $\gamma_y = \partial z / \partial y$ the slope along $\hat{\mathbf{y}}$. Σ_{PO} is the target illuminated surface. The incidence and observation propagation vectors directions are defined with the Forward Scattering Alignment convention. $\bar{\mathbf{a}}_1$, $\bar{\mathbf{a}}_2$ and $\bar{\mathbf{a}}_3$ matrices depend on the incidence angles (θ_i, ϕ_i) and observation angles (θ_s, ϕ_s):

$$\bar{\mathbf{a}}_1 = \begin{bmatrix} \sin\theta_s \cos\phi_i & a_{1_{\theta\phi}} \\ 0 & \sin\theta_i \cos\phi_s \end{bmatrix} \tag{2}$$

$$\bar{\mathbf{a}}_2 = \begin{bmatrix} \sin\theta_s \sin\phi_i & a_{2_{\theta\phi}} \\ 0 & \sin\theta_i \sin\phi_s \end{bmatrix} \tag{3}$$

$$\bar{\mathbf{a}}_3 = \begin{bmatrix} -\cos\theta_s \cos\phi_{si} & -\cos\theta_s \cos\theta_i \sin\phi_{si} \\ \sin\phi_{si} & -\cos\theta_i \cos\phi_{si} \end{bmatrix} \tag{4}$$

with $a_{1_{\theta\phi}} = \cos\theta_s \sin\phi_s \sin\theta_i - \cos\theta_i \sin\phi_i \sin\theta_s$, $a_{2_{\theta\phi}} = \cos\theta_i \cos\phi_i \sin\theta_s - \cos\theta_s \cos\phi_s \sin\theta_i$, and $\phi_{si} = \phi_s - \phi_i$. Scalars b_1, b_2 and b_3 are functions of the incidence $\hat{\mathbf{k}}_i$ and observation $\hat{\mathbf{k}}_s$ propagation vectors:

$$b_1 = k_0(-\sin\theta_i \cos\phi_i + \sin\theta_s \cos\phi_s) \tag{5}$$

$$b_2 = k_0(-\sin\theta_i \sin\phi_i + \sin\theta_s \sin\phi_s) \quad (6)$$

$$b_3 = k_0(-\cos\theta_i + \cos\theta_s) \quad (7)$$

The PO approximation validity domain is:

- $L \gg \lambda$, with L the object size and λ the wavelength (*high-frequency assumption*),
- $R_c \gg \lambda$, for moderate local incident angles, with R_c the radius of curvature of the surface (*tangent plane approximation*).

The illuminated object RCS can be obtained from the diffraction matrix by:

$$\bar{\boldsymbol{\sigma}} = \lim_{R'\to\infty} 4\pi R'^2 \begin{bmatrix} |S_{\theta\theta}|^2 & |S_{\theta\phi}|^2 \\ |S_{\phi\theta}|^2 & |S_{\phi\phi}|^2 \end{bmatrix} \quad (8)$$

Equations (1) and (8) make it possible to calculate the RCS of a surface with any height profile $z(x, y)$, but require 2 numerical integrations. This can lead to long computing times for large surface areas with respect to the squared wavelength. Indeed, a surface sampling step of tenth the wavelength is necessary to get a satisfactory calculation accuracy.
For a smooth plate, $z = 0$ and $\gamma_x = \gamma_y = 0$, Eq. (1) is reduced to $\bar{\mathbf{S}} = P\bar{\mathbf{a}}_3 \int\int e^{i(b_1x+b_2y)}dxdy$ and an analytical solution is obtained for canonical shapes of the surface:

- For a rectangular plate with lengths L_x and L_y:

$$\bar{\mathbf{S}} = P\bar{\mathbf{a}}_3 L_x L_y \mathrm{sinc}\left(\frac{L_x b_1}{2}\right) \mathrm{sinc}\left(\frac{L_y b_2}{2}\right) \quad (9)$$

- For a circular plate with radius a and $\beta = \sqrt{b_1^2 + b_2^2}$:

$$\bar{\mathbf{S}} = P\bar{\mathbf{a}}_3 \pi a^2 \frac{2\mathrm{J}_1(a\beta)}{a\beta} \quad (10)$$

with J_1 the Bessel function of the first kind and order 1.

The next two paragraphs detail different approaches, based on the PO approximation, to calculate the RCS of a rough surface. They are summarized in Table IV at the end of paragraph IV.

III. Statistical global approach

This approach consists in estimating the diffraction matrix of a generated random rough surface by its ensemble average $\langle \bar{\mathbf{S}} \rangle$. Indeed, for a random rough surface, the height profile $z(x, y)$ is a random variable together with γ_x and γ_y, and $\langle \bar{\mathbf{S}} \rangle$ is obtained from Eq. (1):

$$\langle \bar{\mathbf{S}}_{rough} \rangle = P \iint e^{i(b_1x+b_2y)} (\underbrace{m_1\bar{\mathbf{a}}_1 + m_2\bar{\mathbf{a}}_2 + m_3\bar{\mathbf{a}}_3}_{\bar{\mathbf{C}}_r}) dxdy \quad (11)$$

with $m_1 = \langle \gamma_x e^{ib_3z} \rangle$, $m_2 = \langle \gamma_y e^{ib_3z} \rangle$, $m_3 = \langle e^{ib_3z} \rangle$ and $\bar{\mathbf{C}}_r$ a roughness coefficient (matrix).

A. Approach 3_1: Analytical statistical approach

m_1, m_2 et m_3 mean values can be calculated analytically from the surface statistical properties. Given that the statistical correlation between z and its slopes equals zero: $\langle z\gamma_{x,y} \rangle = 0$, we have $p_{z,\gamma_x}(z, \gamma_x) = p_z(z)p_{\gamma_x}(\gamma_x)$ and same for γ_y. In addition, $\langle z \rangle = 0 \Rightarrow \langle \gamma_x \rangle = 0$, leading to

$$m_1 = \int_{-\infty}^{\infty} p_z(z) e^{ib_3z} dz \underbrace{\int_{-\infty}^{\infty} p_{\gamma_x}(\gamma_x)\gamma_x d\gamma_x}_{=0} = 0.$$

In the same way, $m_2 = 0$ and

$$\begin{aligned} m_3 &= \langle e^{ib_3z} \rangle = \int_{-\infty}^{\infty} p_z(z) e^{ib_3z} dz \\ &= \int_{-\infty}^{\infty} \frac{1}{\sigma_z\sqrt{2\pi}} e^{-\frac{z^2}{2\sigma_z^2}} e^{ib_3z} dz = e^{-\frac{b_3^2\sigma_z^2}{2}}. \end{aligned} \quad (12)$$

Thus, the statistical average of the diffraction matrix of the rough surface, $\langle \bar{\mathbf{S}}_{rough} \rangle$, is equal to the diffraction matrix of a smooth surface $\bar{\mathbf{S}}_{smooth}$ (given by Eq. (9) for a rectangular plate and Eq. (10) for a circular plate) multiplied by a corrective factor m_3, which is given for Gaussian height PDF by:

$$\langle \bar{\mathbf{S}}_{rough} \rangle = e^{-\frac{b_3^2\sigma_z^2}{2}} \times \bar{\mathbf{S}}_{smooth} \quad (13)$$

The corrective factor m_3 has an analytical expression under the assumption of an infinite rough surface area (or large lengths with respect to the surface height correlation lengths).

B. Approach 3_2 : Numerical statistical approach

In the previous approach, calculation of averages m_1, m_2 and m_3 was performed analytically. In this second statistical approach, these coefficients are calculated numerically from a realization of the surface height $z(x, y)$. In this case:

$$\langle \bar{\mathbf{S}}_{rough} \rangle = \bar{\mathbf{C}}_r P \underbrace{\iint e^{i(b_1x+b_2y)} dxdy}_{calculated\ by\ (9)\ and\ (10)} \quad (14)$$

with the roughness coefficient $\bar{\mathbf{C}}_r = m_1\bar{\mathbf{a}}_1 + m_2\bar{\mathbf{a}}_2 + m_3\bar{\mathbf{a}}_3$ considered as independent of x and y on the surface.

The two developed statistical approaches lead to an analytical expression of the double integral that lies in the expression of the rough surface RCS.

C. Statistical approaches results

Figure 1 shows the bistatic RCS of Rough Sample 1 versus the observation angle θ_s, calculated by the two statistical approaches previously described (analytical and numerical), and compared to the results obtained by the numerical PO method and the reference one (commercial code MLFMM from FEKO). The frequency is 5 GHz, the incidence is normal and the polarisation is $\theta\theta$ (or vertical). The considered Rough Sample 1 is defined in Tables I and II. The developed numerical PO method shows a good agreement with the reference method; differences are noticeable for incidence angles superior to $\pm 40°$, which can be explained by edge

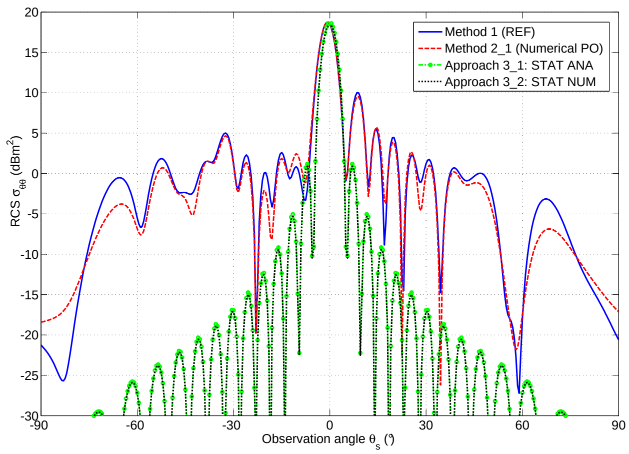

Fig. 1. Bistatic RCS of Sample 1 at 5 GHz, at normal incidence and in $\theta\theta$ (or VV vertical-vertical) polarization, computed from: Method 1 (FEKO MLFMM used as reference), Method 2_1 (numerical PO), Approach 3_1 (analytical statistical) and Approach 3_2 (numerical statistical).

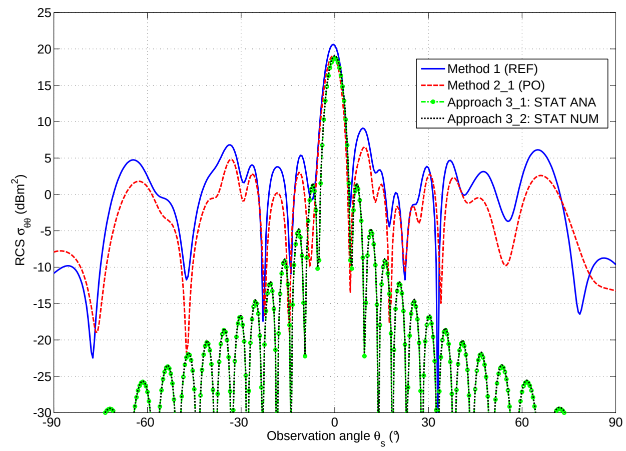

Fig. 2. Bistatic RCS of Sample 2 at 5 GHz, at normal incidence and in $\theta\theta$ (or VV vertical-vertical) polarization, computed from: Method 1 (FEKO MLFMM used as reference), Method 2_1 (numerical PO), Approach 3_1 (analytical statistical) and Approach 3_2 (numerical statistical).

diffraction that PO does not take into account. Figure 2 shows the same variations as figure 1 but for Rough Sample 2, having an exponential autocorrelation function. Larger differences are observed between the RCS calculated by PO and the reference method on this sample, even for small observation angles. Indeed, this surface has high frequency components, contributing outside the specular direction, which are not taken into account by PO.

It is obvious that the developed statistical approaches, approach 3_1 as well as approach 3_2, do not correctly estimate the surface RCS. The assumption consisting in estimating a rough surface RCS by its statistical average (Eq. (11)) is then not validated here. In Eq. (11), for each surface's point, the height z depends on its position (x, y). Thus, the surface double integration and the one corresponding to the statistical mean cannot be inverted. Although the surface is generated with a random height profile z, the calculation is only made on one realization of this process. In addition, the surface length with respect to the surface correlation length is not large enough to fully represent the statistical process. Therefore, statistical operations are not applicable.

For such a study case, the numerical PO requires typically 100 times less computing time than MLFMM to calculate the bistatic RCS between $-90°$ and $+90°$ by $0.5°$ steps (3.07 s and 3.15 s required by PO for samples 1 and 2 respectively against 286 s and 358 s with MLFMM); the acceleration factor is greater and varies between 2000 and 4000 when a monostatic simulation is performed, depending on the rough surface sample provided in Table I.

IV. Deterministic approach: Surface decomposition into cosine components

The presented statistical approach being not suitable to calculate the RCS of the random rough surfaces considered here, the study was oriented towards a deterministic one.

Following [9], the surface height profile $z(x, y)$ can be written as a double sum of sinusoidal components from its height spectrum:

$$
\begin{aligned}
z(x,y) &= \sum_{m=1}^{M-1}\sum_{n=1}^{N-1}\sqrt{2S_z(k_{x_m},k_{y_n})\Delta k_x\Delta k_y} \\
&\quad \times \cos\left(xk_{x_m}+yk_{y_n}+\Phi_{m,n}\right) \qquad (15)\\
&= \sum_{m,n} A_{m,n}\cos\left(xk_{x_m}+yk_{y_n}+\Phi_{m,n}\right) \qquad (16)
\end{aligned}
$$

where Φ_{mn} is a random phase uniformly distributed between 0 and 2π; $\Delta k_x = 2\pi/L_x$ and $\Delta k_y = 2\pi/L_y$ with L_x and L_y the surface lengths along $\hat{\mathbf{x}}$ and $\hat{\mathbf{y}}$ directions, respectively. $A_{m,n}$ is the sinusoid magnitude and k_{x_m} and k_{y_n} are the wavenumbers along $\hat{\mathbf{x}}$ and $\hat{\mathbf{y}}$, respectively.

For the surfaces defined in Table I, wavenumbers k_{x_m} range from $-(\pi/L_x n_x)(n_x+1)/(n_x-1)$ to $+\pi/L_x n_x$, with L_x the surface dimension (here 0.8 m) and n_x the number of surface samples along $\hat{\mathbf{x}}$ direction. n_x shall be chosen such that the surface sampling step, given by the ratio $\Delta_x = L_x/n_x$, must not be greater than a tenth of the smallest incident field wavelength. In this study, the frequency ranges from 2 GHz to 18 GHz, and the rough surface samples have been generated with $n_x = 2^9 = 512$ samples. The power of two just superior to the minimum required number of samples has been chosen, given that an FFT algorithm is used for the surface generation. The derivation is identical along $\hat{\mathbf{y}}$ direction.

To obtain a simple closed-form of Eq. (1), it is assumed that $\gamma_x \approx 0$ and $\gamma_y \approx 0$. It can be shown that this assumption is valid for the surfaces considered in this study. Figure 3 illustrates it: the Sample 3 monostatic RCS computed by the numerical PO (method 2_1) and by the approach called "numerical neglected slopes PO" (approach 2_2) are compared to the RCS computed by the reference method 1. The RCS obtained by the "numerical neglected slopes

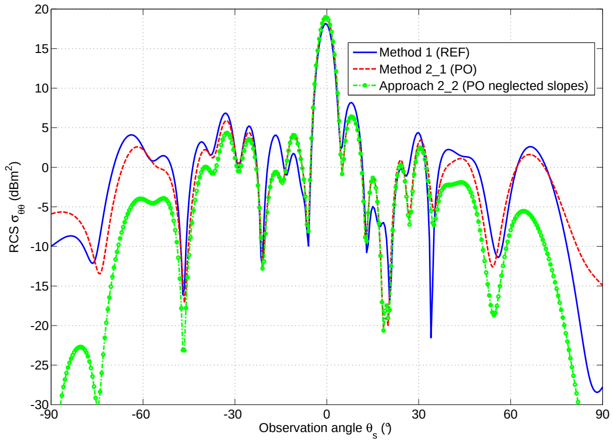

Fig. 3. Monostatic RCS of Sample 3 at 5 GHz and in $\theta\theta$ polarization calculated by: Method 1 (FEKO MLFMM used as reference), Method 2_1 (numerical PO) and Approach 2_2 ("numerical neglected slopes PO").

PO" approach shows differences with the one calculated by numerical PO at angles where the numerical PO itself already starts to deviate from the reference method 1. A specific work has been dedicated to the term involving the surface slopes, but it is not presented in this paper. Accounting for the surface slopes led to add two terms to the "neglected slopes case", each one requiring only one numerical integration. Numerical simulations showed that the term involving the surface slopes was negligible in the frame of this study. In the PO approximation validity domain, and for the surfaces considered in this study (Table I), numerical PO can be approximated by the approach called "numerical neglected slopes PO" and method 2_1 will be replaced by approach 2_2.

If the surfaces slopes are neglected, Eq. (1) reduces to:

$$\bar{\mathbf{S}} = P\bar{\mathbf{a}}_3 \underbrace{\int\int_{\Sigma_{PO}} e^{i(b_1x+b_2y+b_3z(x,y))}dxdy}_{I_3} \tag{17}$$

For a circular plate of radius a in a cylindrical coordinates system, integral I_3 can be written as:

$$\begin{aligned} I_3 &= \int_0^{2\pi}\int_0^a e^{ir\alpha\cos(\theta-\chi)} \\ &\quad\times \prod_{m,n} e^{ib_3A_{m,n}\cos[\beta_{m,n}r\cos(\theta-\gamma_{m,n})+\phi_{m,n}]}rdrd\theta \end{aligned} \tag{18}$$

with:

$$\alpha = \sqrt{b_1^2+b_2^2} \tag{19}$$

$$\chi = \arctan\left(\frac{b_2}{b_1}\right) \tag{20}$$

$$\beta_{m,n} = \sqrt{k_{x_m}^2+k_{y_n}^2} \tag{21}$$

$$\gamma_{m,n} = \arctan\left(\frac{k_{y_n}}{k_{x_m}}\right) \tag{22}$$

A. Approach 4_1 : Semi-analytical θ cosine approach

For the Approach 4_1, the integration over r is derived analytically, whereas the one over θ is computed numerically. Using Bessel functions properties [10]:

$$e^{i\xi\cos(\theta-\varphi)} = \sum_{p=-\infty}^{+\infty} i^p J_p(\xi)e^{ip(\theta-\varphi)} \tag{23}$$

and after developments detailed in Appendix A, I_3 is written as:

$$\begin{aligned} I_3 &= (ia)\prod_{m,n}\sum_{p_{m,n}=-\infty}^{+\infty}\left[i^{p_{m,n}}J_{p_{m,n}}(b_3A_{m,n})e^{ip_{m,n}\phi_{m,n}}\right] \\ &\quad\times\int_0^{2\pi}\frac{e^{iK(\theta)a}}{K(\theta)}\left[-1+e^{-i\frac{K(\theta)a}{2}}\operatorname{sinc}\left(\frac{K(\theta)a}{2}\right)\right]d\theta \end{aligned} \tag{24}$$

with:

$$K(\theta) = \alpha\cos(\theta-\chi)+\sum p_{m,n}\beta_{m,n}\cos(\theta-\gamma_{m,n}). \tag{25}$$

B. Approach 4_2: Semi-analytical r cosine approach

For the Approach 4_2, the integration over θ is derived analytically, whereas the one over r is computed numerically. Using Bessel functions properties, and following the calculation derived in Appendix B, I_3 is written as:

$$\begin{aligned} I_3 &= 2\pi\sum_{k=-\infty}^{+\infty}\prod_{m,n} \\ &\quad\sum_{p_{m,n}=-\infty}^{+\infty}\left[i^{p_{m,n}}J_{p_{m,n}}(b_3A_{m,n})e^{ip_{m,n}\phi_{m,n}}\right] \\ &\quad\times\sum_{\substack{l_{m,n}=-\infty \\ \sum l_{m,n}=-k}}^{+\infty} e^{-i(k\chi+\sum l_{m,n}\gamma_{m,n})} \\ &\quad\times\int_0^a J_k(r\alpha)\left[J_{l_{m,n}}(p_{m,n}\beta_{m,n}r)\right]rdr \end{aligned} \tag{26}$$

Using these last two approaches, the calculation of I_3 requires only one numerical integration over θ or r. Infinite sums of Bessel functions appear in the obtained expression of I_3; the required rank for the series convergence will then be studied.

It can be noted that, in cases where the series convergence is obtained for the summation rank 0, the expression of I_3 (Eq. (26)) is simplified. Only Bessel functions of order 0, J_0, are taken into account in the calculation. An analytical solution, which involves the expression of a circular smooth plate, is then obtained. This corresponds to the approach called Approach 4_2_N:

$$I_3 = \underbrace{\frac{2\pi a}{\alpha}J_1(a\alpha)}_{smooth}\prod_{m,n}J_0(b_3A_{m,n}) \tag{27}$$

C. Numerical results

1) Surface made of 1 cosine component: First, the considered surface is made of only one cosine component: $z(x, y) = A_1 \cos(k_{x_1} x + k_{y_1} y + \Phi_1)$. In this case, I_3 expressions are:

- Approach 4_1_1:

$$
\begin{aligned}
I_3 &= ia \sum_{p_1=-\infty}^{+\infty} i^{p_1} J_{p_1}(b_3 A_1) e^{i^{p_1 \phi_1}} \qquad (28)\\
&\times \int_0^{2\pi} \frac{e^{iK_1 a}}{K_1} \left[-1 + e^{-i\frac{K_1 a}{2}} \operatorname{sinc}\left(\frac{K_1 a}{2}\right) \right] d\theta
\end{aligned}
$$

  with $K_1 = \alpha \cos(\theta - \chi) + p_1 \beta_1 \cos(\theta - \gamma_1)$.
- Approach 4_2_1:

$$
\begin{aligned}
I_3 &= 2\pi a \sum_{k=-\infty}^{+\infty} (-1)^k e^{-ik(\chi - \gamma_1)}\\
&\times \sum_{p_1=-\infty}^{+\infty} \frac{i^{p_1}}{\alpha^2 - (p_1\beta_1)^2} J_{p_1}(b_3 A_1) e^{i^{p_1 \phi_1}}\\
&\times [\alpha J_{k+1}(\alpha a) J_k(p_1 \beta_1 a)\\
&-p_1 \beta_1 J_k(\alpha a) J_{k+1}(p_1 \beta_1 a)] \qquad (29)
\end{aligned}
$$

In this case, the integration over r is also done analytically from [11] and I_3 has an analytical expression.
The summation indexes P_1 and K (p_1 varies from -P_1 to P_1 and k from -K to K) at which convergence occurs are investigated. A sensitivity study on the magnitude parameter A_1 and wavenumber k_{x_1} reveals that:

- for a given surface sinusoid wavenumber, larger its amplitude, larger summation orders P_1 and K are required to get convergence towards the "numerical neglected slopes PO" approach;
- for a given surface sinusoid amplitude, smaller its wavenumber, larger summation orders P_1 and K are required to get convergence towards the "numerical neglected slopes PO" approach.

Figure 4 shows the bistatic RCS of a surface made of 1 cosine component, calculated by both the cosine approaches and the "numerical neglected slopes PO" approach, versus the observation angle θ_s. The frequency is 5 GHz, the incidence is normal, the cosine component amplitude is $A_1 = 0.75$ cm and its wavenumber is $k_{x_1} = k_{y_1} = 2\pi/L$, with L the surface diameter equal to 0.8 m, and phase $\phi_1 = 0°$. These surface parameters have been chosen to highlight the impact of K and P_1 indexes on the RCS calculation. Indexes $K = 4$ and $P_1 = 1$ shall be reached to get the analytical cosine approach 4_2_1 to converge towards the "numerical neglected slopes PO" approach (approach 2_2). Similar results are obtained with the semi-analytical θ cosine approach 4_1_1, with convergence occurring for $P_1 = 1$. The RCS calculated by the reference method has not been added in the figure for the sake of clarity; however, a good correspondence between the "numerical neglected slopes PO" approach (approach 2_2) and reference (method 1) is observed up to 40° (1 dB RCS difference between both methods reached at 41° observation).

For this study case, the computing times required to get the bistatic RCS from 0° to 90° by 0.5° steps on a 3 GHz frequency PC with 4 Go RAM are:

- more than 2.25 hours with MLFMM,
- 27 s with "numerical neglected slopes PO" approach 2_2,
- 0.25 s with the semi-analytical θ cosine approach 4_1_1 (convergence for $P_1 = 1$),
- 0.09 s with the analytical cosine approach 4_2_1 (convergence for $K = 4$ and $P_1 = 1$).

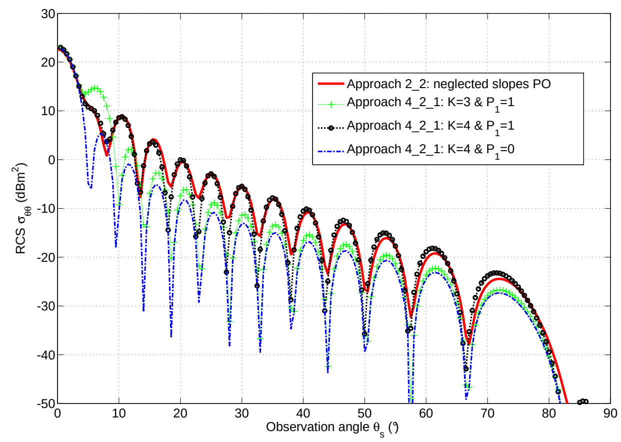

Fig. 4. Bistatic RCS at 5 GHz of the selected surface made of 1 cosine calculated with the "numerical neglected slopes PO" approach and analytical cosine approach 4_2_1 for different summation indexes values.

It shall be noted that this case is more restrictive than the surfaces considered in this study, for which convergence is reached for $P_1 = 0$ or $K = P_1 = 0$ (contribution of Bessel function of order 0: J_0 only) for all (A_1, $k_{x_1} = k_{y_1}$) pairs checking Eq. (16) and parameters defined in Tables I and II. The computing time speed-up is even higher for these cases: a gain factor larger than 200 with approach 3 and 500 with approach 4 are obtained with respect to the "numerical neglected slopes PO" approach.

2) Surface made of the sum of $M \times N$ cosine components: Considering the promising results obtained on a surface made of one cosine component, the generalization to the $M \times N$ components was first undertaken using the analytical Approach 4_2_N, which only involves the contribution of the Bessel functions of order 0: J_0. Unfortunately, this approach only predicts RCS of surfaces very close to a smooth plate. Indeed, its expression (Eq. (27)) involves a product of Bessel functions of order 0 and argument $b_3 A_{m,n}$, where $A_{m,n}$ is the amplitude of the cosine components. J_0 function is maximum for a null argument and decreases rapidly when its argument increases. Thus, the contribution of J_0 functions is significant only for small $A_{m,n}$ values; that is to say surfaces like a smooth plate. Moreover, the cosine components wavenumber k_{x_m} and k_{y_n} do not appear in Eq. (27). Approach 4_2_N is then not suitable to evaluate the RCS of the surfaces considered in this study.

Complexity analysis: To treat the general case of $M \times N$ cosine components, Approach 4_1, defined by equation (24), was selected rather than Approach 4_2, defined by equation (26). Indeed, in equation (26), the infinite series indexes are related to each other $\sum_{k=-\infty}^{+\infty} \cdots \sum_{l_{m,n}=-\infty}^{+\infty} \cdots$ with $\sum l_{m,n} = -k$, which makes the programming of this equation complicated. Complexity inherent to equation (24) can be expressed by: $n_u \times (2P_1 + 1)^{M \times N}$, where n_u is the number of unknowns along one dimension x or y. By comparison, numerical PO complexity is n_u^2. Thus:

- if convergence occurs for $P_1 = 1$, Approach 4_1 complexity is lower than the numerical PO one for $M \times N < 5$,
- if convergence occurs for $P_1 = 2$, Approach 4_1 complexity is lower than the numerical PO one for $M \times N < 3$.

In comparison, the rigorous MoM requires n_u^2 scaling of memory requirements (to store the impedance matrix) and n_u^3 in CPU-time (to solve the linear set of equations). The MLFMM formulation's more efficient treatment of the same problem results in $n_u \log(n_u)$ scaling in memory and $n_u \log(n_u) \log(n_u)$ in CPU time.

Approach 4_1 is thus only useful for a small number of surface constitutive cosine components, which corresponds to restrictive cases in terms of generated surface diversity. However, some cosine components can be neglected without noticeable degradation of the RCS estimation, and this approach makes it possible to determine how the different surface spectrum frequencies contribute to the surface RCS. The selected surface to compare the different approaches is made of 5 cosine components; its constitutive wavenumbers k_{x_m} are: $2\pi/L_x \times \{1; n_x/2^7; n_x/2^5; n_x/2^3; n_x/2\}$ and $k_{y_n} = 2\pi/L_y$, with $L_x = L_y = L = 0.8$ m and $n_x = 2^9$. These surface's parameters are shown in Table III.

Shape	Diameter	σ_z	σ_{γ_x}	σ_{γ_y}
Circle	80 cm	0.99 cm	0.1	0.08

TABLE III
5 COSINE COMPONENTS SURFACE PARAMETERS.

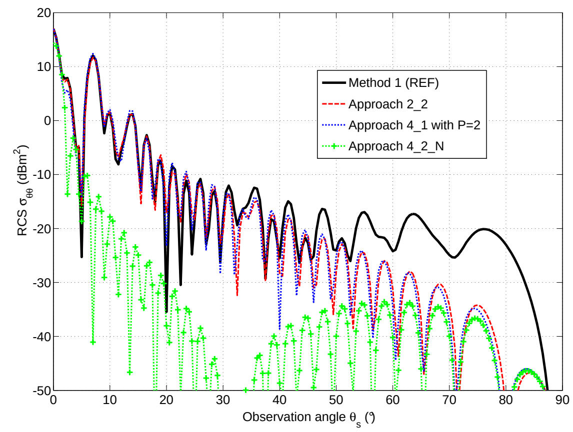

Fig. 5. Monostatic RCS at 5 GHz of the selected surface made of 5 cosine components calculated with FEKO, "numerical neglected slopes PO", Approach 4_1 with $P = 2$, and Approach 4_2_N.

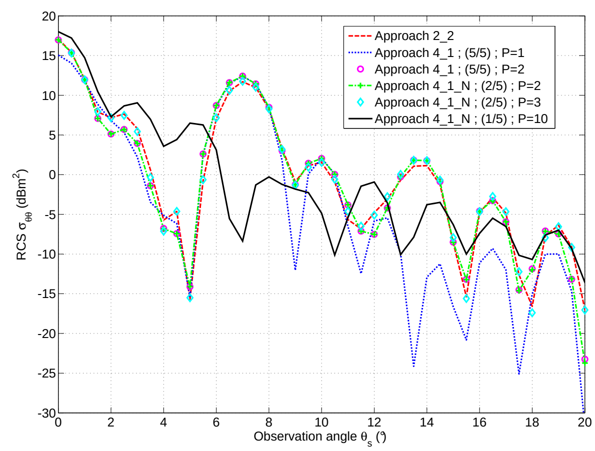

Fig. 6. Monostatic RCS at 5 GHz of the selected surface made of 5 cosine components calculated with the "numerical neglected slopes PO" approach and Approach 4_1 for different summation indexes P and different numbers of constitutive cosine components accounted for in the calculation.

Figure 5 shows this surface monostatic RCS calculated with Method 1 (reference), Approach 2_2 ("numerical neglected slopes PO"), cosine Approach 4_1 (one numerical integration) with $P = 2$, and analytical cosine approach 4_2_N. Approach 4_1 has converged towards the "numerical neglected slopes PO" approach for the summation index $P = 2$ and, like PO, shows a good agreement with reference Method 1 up to observation angles around 40°. This figure also illustrates that analytical Approach 4_2_N does not correctly estimate the RCS of such surfaces. Approach 4_1 for 5 cosine components with summation index $P = 2$ has a higher complexity than numerical PO; however, taking only the two highest amplitudes cosine components among the five constitutive ones into account, in the RCS calculation using Approach 4_1, is sufficient to get a good estimation of the surface RCS.

Computing times required by the different approaches to calculate the monostatic RCS of the 5 cosine components surface between 0 and 90° by 0.5° steps are shown in Table V. NC in front of the computing time means that the method did not converge towards the "numerical neglected slopes PO" approach for the corresponding summation index P.

Figure 6 shows the 5 cosine components surface monostatic RCS, calculated by several approaches, versus the observation angle θ_s. A zoom on the $[0°, 20°]$ angular range is done in this figure, where differences between the curves can be seen. The compared approaches are Approach 2_2 ("numerical neglected slopes PO") and Approach 4_1 considering all the 5 cosine components (for $P = 1$ and $P = 2$), 2 of the 5 (the two having highest amplitude) cosine components (for $P = 2$ and $P = 3$), and only one of the 5 cosine components (for $P = 2$ and $P = 10$). When only the highest amplitude cosine component is taken into account in the RCS calculation, the RCS obtained by Approach 4_1 never converges towards the RCS obtained by the "numerical neglected slopes PO" approach, even for high values of the summation index P. Accounting for only one, the highest amplitude one, cosine component composing this surface to calculate its RCS is not sufficient to correctly estimate this surface RCS. However, results from Approach 4_1, which considers only 2 of the 5 cosine components, are merged with those obtained with the complete constitutive components for $P \geq 2$. This surface RCS can thus be estimated by accounting for only 2 of its 5 constitutive components, the 2 having highest amplitudes. This surface spectrum can thus be truncated in the RCS calculation and the RCS calculation simplified, without noticeable degradation of its RCS results. This simplified calculation is a bit more rapid than the "numerical neglected slopes PO" approach in this case; unfortunately, the acceleration factor is not significant.

Attempts have been made to modify Eq. (24) by simplifying the calculation of factor $K(\theta)$, and lower Approach 4_1 complexity but their results were not satisfactory; however, this work is on-going and is part of the prospects of this paper, as well as simplifying Eq. (26).

Approach $no.$	Approach name	Equation
1	MLFMM FEKO (reference)	
2_1	Numerical PO	(1)
2_2	Numerical neglected slopes PO	(17)
3_1	Analytical statistical approach	(13)
3_2	Numerical statistical approach	(14)
4_1	Semi-analytical-θ cosine approach	(24)
4_2	Semi-analytical-r cosine approach	(26)
4_1_1	Semi-analytical-θ 1-cosine approach	(28)
4_2_1	Analytical 1-cosine approach	(29)
4_2_N	Analytical N J_0 cosine approach	(27)

TABLE IV
APPROACHES USED TO CALCULATE THE SURFACE RCS.

Approach	Configuration	Index	Computing time
Method 1			7481 s
Approach 2_2			30 s
Approach 4_2_N			NC
Approach 4_1	5/5 cosine	P=1	NC
Approach 4_1	5/5 cosine	P=2	3076 s
Approach 4_1	2/5 cosine	P=1	NC
Approach 4_1	2/5 cosine	P=2	22 s
Approach 4_1	2/5 cosine	P=3	33 s
Approach 4_1	1/5 cosine	P=2	NC
Approach 4_1	1/5 cosine	P=10	NC

TABLE V
COMPARISON OF THE APPROACHES COMPUTING TIMES.

V. RCS MEASUREMENTS

The samples RCS measurements were a key point of this project to get a validation of the various codes. However, these large samples RCS measurements over a wide frequency band are challenging and the experimental measurements configuration was very critical.
The three samples with profiles defined in Table I, as well as a smooth plate of diameter 80 cm, have been machined from aluminum cylinders (Fig. 7), by Bretagne Usinage Grande Vitesse company. Their RCS have been measured from 2 GHz to 18 GHz, in CHEOPS anechoic chamber at DGA, Bruz, in January 2012. To be measured, the samples were placed on the top of a Styrofoam mast, hung by a sling, in the anechoic chamber. The measurement configuration is quasi-monostatic (there are two antennas: one for transmission and one for reception but they are placed very close together). The distance between the antennas and the sample is 17.9 m, which ensures the far-field criterion of $2L^2/\lambda$, with L the largest sample dimension (diameter of 80 cm), up to 4.2 GHz. The samples RCS measurements are calibrated by 22.5° inclined dihedral ones; the far-field effects (distance and sphericity) are corrected as well as the transmitting and receiving antennas positions. In each frequency band and for each sample, the 4 polarisations have been measured ($\theta\theta$ and $\theta\phi$, then $\phi\phi$ and $\phi\theta$). The measured angle range is -50° to +50°.

A. Circular smooth plate RCS measurements

This reference plate is flat within the mechanical machining precision. It is circular, its diameter is 800 mm, its thickness 8 mm and its edges are chamfered to limit their diffraction contribution. Figure 8 shows the smooth plate RCS at normal incidence versus frequency: the measurements with and without far-field corrections are shown, as well as the far-field calculation (numerical PO) and near-field calculation ([12],[13]). In high frequency (f > 8 GHz), it can be noted that the agreement of the near-field (uncorrected) measurements with the near-field simulation is better than the agreement of the far-field (corrected) measurements with the far-field simulation. This can be explained by the correction applied on the measurements. The far-field correction is only partial, because it can only be applied in the scan plane, that is to say the horizontal one. The raw measurements (without far-field correction) show a very good agreement with near-field numerical PO over the whole measured bandwidth. Remaining differences can be explained as follows:

- the observed ripples for varying frequency in S band ([2 - 4 GHz]) are due to the calibration on the dihedral,
- in Ku band ([12 - 18 GHz]), positioning the large smooth plate on the Styrofoam mast is critical; the 3 dB beam is very narrow (around 0.5°) and a slight elevation angle positioning error strongly decreases the measured response. This mechanical difficulty causes the measurements underestimation for high frequencies.

The perfect measurement/simulation match in C-band ([4 - 8 GHz]) can also be observed in Fig. 9, which shows the smooth plate RCS at 5 GHz versus the observation angle, obtained by measurement, by computing with MLFMM and computing with numerical PO.

B. Rough surface samples RCS measurements

Positioning the 80 cm-diameter and 50 kg rough surfaces samples on the top of the Styrofoam mast was also critical, and the RCS measurements azimuthal angle position needs to be adjusted by post-processing (around 5° difference). For

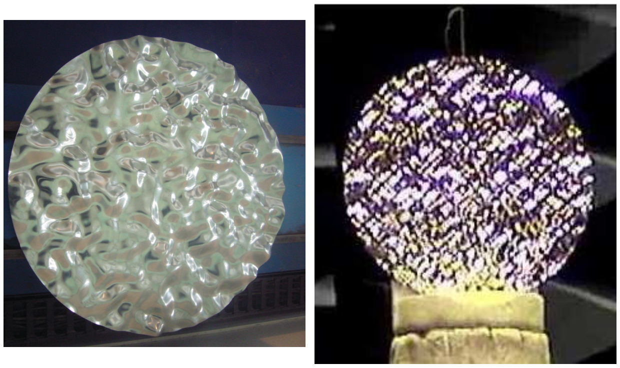

Fig. 7. Built surface samples, on the left: sample 3 (Gaussian autocorrelation function, $L_c = 3$ cm), on the right sample 2 (exponential autocorrelation function, $L_c = 5$ cm) mounted on the Styrofoam mast in the measurement chamber.

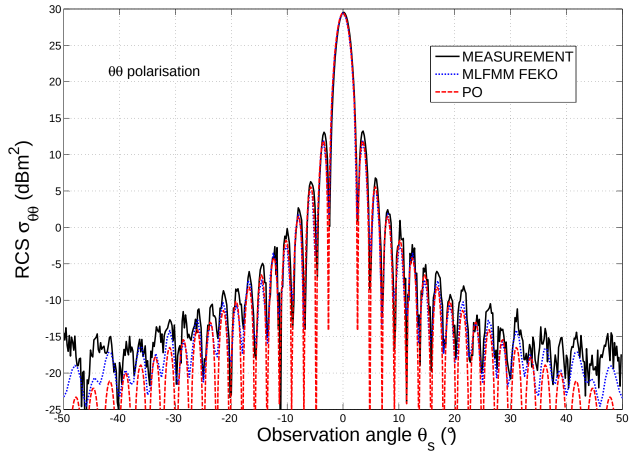

Fig. 9. Smooth plate RCS and phase in $\theta\theta$ polarization at 5 GHz.

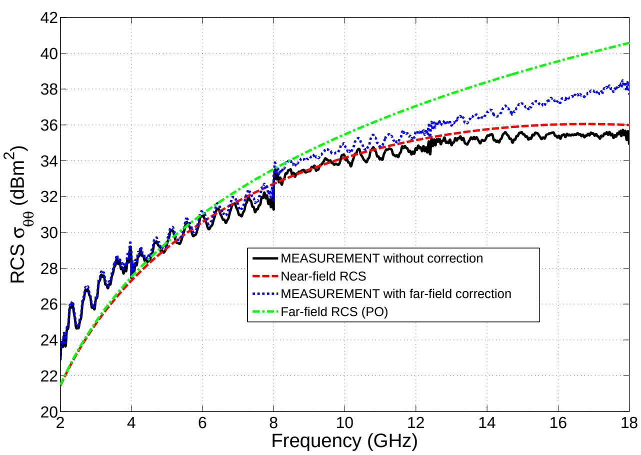

Fig. 8. Smooth plate RCS from 2 to 18 GHz at $\theta_s = 0$: comparison of measurements and simulations in near and far fields.

the rough samples, measurements and theory are also in good agreement. Figure 10 shows sample 3 RCS measured and calculated at 2 GHz in $\theta\theta$ polarisation. Figure 11 shows sample 1 RCS measured and calculated at 5 GHz in $\theta\theta$ and $\theta\phi$ polarisations. The cross-polarisation levels lie around -20 dBm^2, that is to say 40 dB smaller than the co-polarisation ones, and agree well with the ones simulated with MLFMM. PO simulations are only shown for the co-polarisation components, since this method predicts zero for the cross-polarisation ones. At law frequencies, a good match between measurement and simulation is obtained. For sample 2 having an exponential autocorrelation function, which RCS at 5 GHz in $\theta\theta$ polarisation is shown in figure 12, larger differences appear. PO is applicable on the surface having an exponential autocorrelation function but leads to less precise results since the surface high frequency components, contributing outside the specular direction, are not taken into account by PO. An asymptotic model of higher order like Small Slopes Approximation could be used instead of PO to better predict the response of a surface showing small scale, rapid variations. For higher frequencies, above about 6 GHz, the rough samples RCS do not show a main beam in the specular direction anymore, the response being spread in all observation angles directions (see Fig. 13).

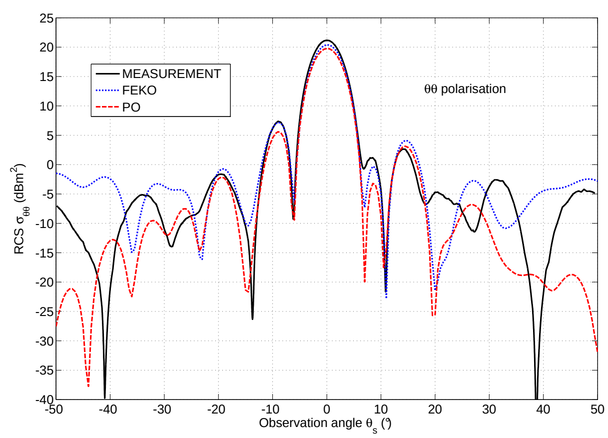

Fig. 10. Rough surface sample 3 RCS in $\theta\theta$ polarization, and at 2 GHz.

VI. Conclusion

Various approaches have been developed in the frame of this study to obtain the RCS of random rough surfaces. The developed method based on PO approximation gives results in good agreement with the MLFMM of FEKO, used as

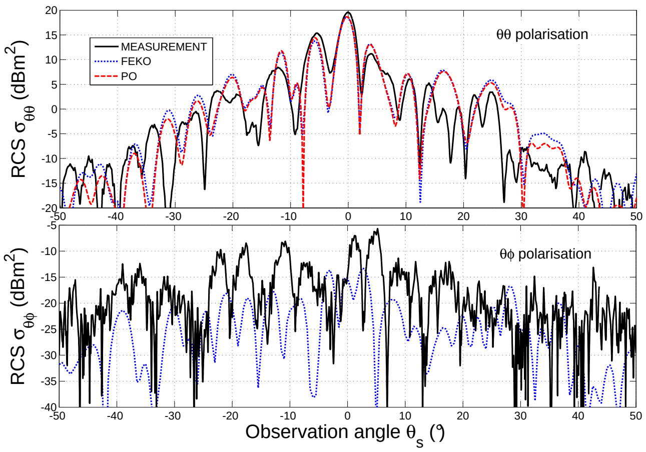

Fig. 11. Rough surface sample 1 RCS in $\theta\theta$ and $\theta\phi$ polarizations, and at 5 GHz.

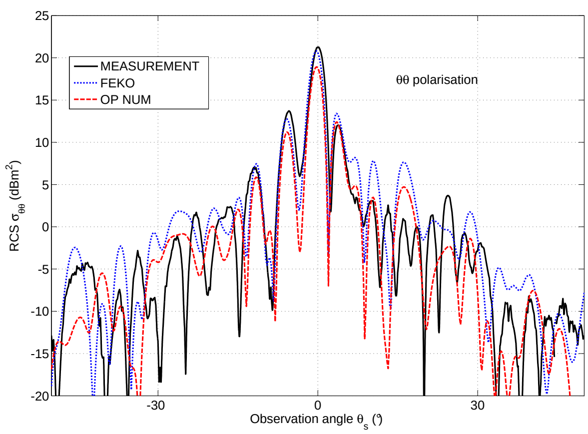

Fig. 12. Rough surface sample 2 RCS in $\theta\theta$ polarization, and at 5 GHz.

reference, for moderate incidence angles, but with an acceleration factor about 100 for a bistatic simulation and about 3000 for a monostatic one. Unfortunately, the undertaken statistical approaches do not correctly estimate the RCS of a given random rough surface. Indeed, the surface is a single realization of the random process that generates it and is not large enough to fully represent the statistical process. The developed deterministic approaches based on the random rough surface decomposition into a sum of cosine components makes it possible to expedite the RCS calculation by a factor 500 when the surface is constituted of only one cosine; and their complexity limits their application to surfaces made of only a few cosine components. However, this approach shows that not all surface spectral components significantly contribute to its RCS, and makes it possible to discriminate the contribution

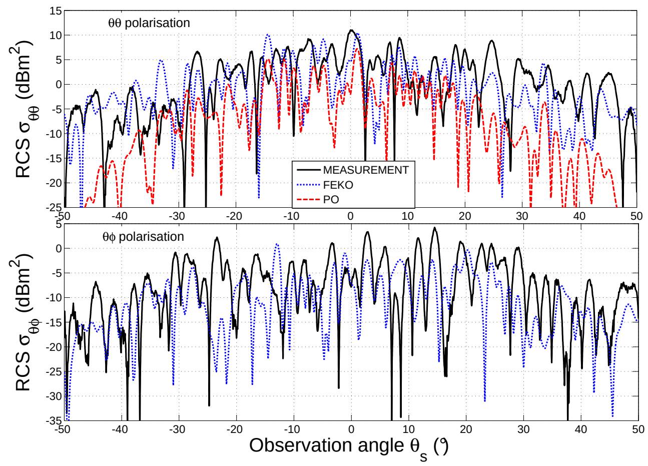

Fig. 13. Rough surface sample 2 RCS in $\theta\theta$ and $\theta\phi$ polarizations, and at 10 GHz.

of these spectral components to the surface RCS. Prospects of this work include looking for wise simplification of these approaches in order to lower their complexity. Measurements on rough surface samples provided results in good agreement with the RCS calculated by MLFMM and PO restricted to its validity domain. It must be highlighted that these RCS measurements are sensitive to the mechanical configuration and that very good care needs to be taken when positioning the samples in the anechoic chamber.

VII. Acknowledgments

This work has been led in the frame of REI POGO DGA contract 2009.34.0053. The authors would like to thank DGA/MI for supporting this study, and in particular A. Menard and his team for performing the RCS measurements.

Appendix A
Approach 4_1 development

$$
\begin{aligned}
I_3 &= \int_0^{2\pi}\int_0^a e^{ir\alpha\cos(\theta-\chi)} \\
&\quad\times\prod_{m,n} e^{ib_3 A_{m,n}\cos[\beta_{m,n} r\cos(\theta-\gamma_{m,n})+\phi_{m,n}]} r dr d\theta \\
&= \int_0^{2\pi}\int_0^a e^{ir\alpha\cos(\theta-\chi)}\prod_{m,n}\sum_{p_{m,n}=-\infty}^{\infty} i^p_{m,n} J_{p_{m,n}}(b_3 A_{m,n}) \\
&\quad\times e^{ip_{m,n}[\beta_{m,n} r\cos(\theta-\gamma_{m,n})+\phi_{m,n}]} r dr d\theta
\end{aligned}
\tag{30}
$$

$$
\begin{aligned}
I_3 &= \prod_{m,n} \sum_{p_{m,n}=-\infty}^{+\infty} \left[i^{p_{m,n}} J_{p_{m,n}}(b_3 A_{m,n}) e^{i^{p_{m,n}\phi_{m,n}}} \right] \\
&\times \int_0^{2\pi} \int_0^a e^{ir[\alpha \cos(\theta-\chi) + \sum p_{m,n}\beta_{m,n} \cos(\theta-\gamma_{m,n})]} r dr d\theta \\
&= \prod_{m,n} \sum_{p_{m,n}=-\infty}^{+\infty} \left[i^{p_{m,n}} J_{p_{m,n}}(b_3 A_{m,n}) e^{i^{p_{m,n}\phi_{m,n}}} \right] \\
&\times \int_0^{2\pi} \int_0^a e^{irK_{m,n}(\theta)} r dr d\theta
\end{aligned}
$$

with:

$$
K_{m,n}(\theta) = \alpha \cos(\theta - \chi) + \sum p_{m,n}\beta_{m,n} \cos(\theta - \gamma_{m,n}) .
$$

$$
\begin{aligned}
I_3 &= \prod_{m,n} \sum_{p_{m,n}=-\infty}^{+\infty} \left[i^{p_{m,n}} J_{p_{m,n}}(b_3 A_{m,n}) e^{i^{p_{m,n}\phi_{m,n}}} \right] \\
&\times \int_0^{2\pi} ia \frac{e^{iK_{m,n}(\theta)a}}{K_{m,n}(\theta)} \\
&\times \left[-1 + e^{-i\frac{K_{m,n}(\theta)a}{2}} \operatorname{sinc}\left(\frac{K_{m,n}(\theta)a}{2} \right) \right] d\theta \\
&= (ia) \prod_{m,n} \sum_{p_{m,n}=-\infty}^{+\infty} \left[i^{p_{m,n}} J_{p_{m,n}}(b_3 A_{m,n}) e^{i^{p_{m,n}\phi_{m,n}}} \right] \\
&\times \int_0^{2\pi} \frac{e^{iK_{m,n}(\theta)a}}{K_{m,n}(\theta)} \\
&\times \left[-1 + e^{-i\frac{K_{m,n}(\theta)a}{2}} \operatorname{sinc}\left(\frac{K_{m,n}(\theta)a}{2} \right) \right] d\theta
\end{aligned}
$$

APPENDIX B
APPROACH 4_2 DEVELOPMENT

$$
\begin{aligned}
I_3 &= \int_0^{2\pi} \int_0^a e^{ir\alpha \cos(\theta-\chi)} \\
&\times \prod_{m,n} e^{ib_3 A_{m,n} \cos[\beta_{m,n} r \cos(\theta-\gamma_{m,n}) + \phi_{m,n}]} r dr d\theta \\
&= \int_0^{2\pi} \int_0^a \sum_{k=-\infty}^{+\infty} i^k J_k(r\alpha) e^{ik(\theta-\chi)} \\
&\times \prod_{m,n} \sum_{p_{m,n}=-\infty}^{\infty} i^{p_{m,n}} J_{p_{m,n}}(b_3 A_{m,n}) \\
&\times e^{ip_{m,n}[\beta_{m,n} r \cos(\theta-\gamma_{m,n}) + \phi_{m,n}]} r dr d\theta
\end{aligned} \tag{31}
$$

$$
\begin{aligned}
I_3 &= \int_0^{2\pi} \int_0^a \sum_{k=-\infty}^{+\infty} i^k J_k(r\alpha) e^{ik(\theta-\chi)} \\
&\times \prod_{m,n} \sum_{p_{m,n}=-\infty}^{\infty} i^{p_{m,n}} J_{p_{m,n}}(b_3 A_{m,n}) e^{ip_{m,n}\phi_{m,n}} \\
&\cdot \sum_{l_{m,n}=-\infty}^{+\infty} i^{l_{m,n}} J_{l_{m,n}}(p_{m,n}\beta_{m,n} r) e^{il_{m,n}(\theta-\gamma_{m,n})} r dr d\theta
\end{aligned} \tag{32}
$$

$$
\begin{aligned}
I_3 &= \sum_{k=-\infty}^{+\infty} \prod_{m,n} \sum_{p_{m,n}=-\infty}^{+\infty} \sum_{l_{m,n}=-\infty}^{+\infty} i^k \\
&\times \left[i^{p_{m,n}} i^{l_{m,n}} J_{p_{m,n}}(b_3 A_{m,n}) e^{ip_{m,n}\phi_{m,n}} \right] \\
&\times \int_0^a J_k(r\alpha) \left[J_{l_{m,n}}(p_{m,n}\beta_{m,n} r) \right] r dr \\
&\underbrace{\times \int_0^{2\pi} e^{ik(\theta-\chi)} \left[e^{il_{m,n}(\theta-\gamma_{m,n})} \right] d\theta}_{2\pi\delta(k+\sum l_{m,n}) e^{-i(k\chi+\sum l_{m,n}\gamma_{m,n})}} \\
&= 2\pi \sum_{k=-\infty}^{+\infty} \prod_{m,n} \sum_{p_{m,n}=-\infty}^{+\infty} \left[i^{p_{m,n}} J_{p_{m,n}}(b_3 A_{m,n}) e^{ip_{m,n}\phi_{m,n}} \right] \\
&\times \sum_{\substack{l_{m,n}=-\infty \\ \sum l_{m,n}=-k}}^{+\infty} e^{-i(k\chi+\sum l_{m,n}\gamma_{m,n})} \\
&\times \int_0^a J_k(r\alpha) \left[J_{l_{m,n}}(p_{m,n}\beta_{m,n} r) \right] r dr
\end{aligned}
$$

REFERENCES

[1] K.F. Warnick and W.C. Chew, *Numerical simulation methods for rough surface scattering*, Waves in Random Media, vol. 11, no. 1, pp.1-30, 2001.

[2] M. Saillard and A. Santenac, *Rigorous solutions for electromagnetic scattering from rough surfaces*, Waves in Random Media, vol. 11, pp. R103-R137, 2001.

[3] T.M. Elfouhaily and C.A. Guerin, *A Critical Survey of approximate Scattering Wave Theories from Random Rough Surfaces*, Waves in Random Media 14, R1-R40, 2004.

[4] F.T. Ulaby, R.K. Moore and A.K. Fung, *Microwave Remote Sensing vol II*, Reading, MA: Addison-Wesley, 1982.

[5] F.T. Ulaby, and C. Elachi, *Radar Polarimetry for Geoscience Application*, Boston, MA: Artech House, 1990.

[6] J.A. Ogilvy, *Theory of wave scattering from random rough surfaces*, Institute of Physics, Bristol, 1991.

[7] P. Beckmann and A. Spizzichino, *The Scattering of Electromagnetic Waves from Rough Surfaces: Part I. Theory*, London: Pergamon, 1963.

[8] M. Kouali, G. Kubické, and C. Bourlier, *Extended propagation-inside-layer expansion method combined with the forward-backward method to study the scattering from an object above a rough surface*, Opt.Lett. 37, 2985-2987, 2012.

[9] C. Bourlier, *Shadowing function with single reflection from anisotropic Gaussian rough surface. Application to Gaussian, Lorentzian and sea correlations*, Waves Random Media 13 (2003) 27-58, November 2002.

[10] M. Abramowitz and I.A. Segun, *Handbook of Mathematical Functions*, New York: Dover, 1972.

[11] I.S. Gradshtteyn, *Table of integrals, series and products*, Academic Press, Sixth Edition.

[12] P. Pouliguen, *Analytical formulae for radar cross section in near field and normal incidence*, Progress In Electromagnetics Research B, Vol. 9, 263-279, 2008.

[13] C. Bourlier, *Useful analytical formulae for near-field monostatic radar cross section under the Physical Optics: far-field criterion*, IEEE Trans. Ant. Prop., vol. 57, no. 1, pp. 205-214, 2009.

Charlotte Corbel was born in Chatenay Malabry, France, in 1980. She received the B.S. degree in engineering from the Ecole Nationale Supérieure des Télécommunications de Bretagne, Brest, France and the M.S. degree in spacecraft technologies and satellite communications from the University College of London, London, U.K., in 2002. From 2003 to 2010, she has been with Centre d'étude des Environnements Terrestre et Planétaires (currently, Laboratoire ATmosphère, Milieux, Observations Spatiales), Vélizy, France, where she worked on radars and radiometer developments and, since 2005, she has been an Instrument Project Manager of the Water Ice and Subsurface Deposit Information On Mars (WISDOM) and the Electromagnetic Investigation of the Subsurface Ground Penetrating Radars proposed on the ExoMars mission. Since 2010, she works at IETR-Nantes in the Teledetection team on rough surfaces electromagnetic modelling and Radar Cross Section measurements.

Christophe Bourlier was born in La Flèche, France on July 6, 1971. He received the M.S. degree in Electronics from the University of Rennes (France), in 1995. While at the University of Rennes, he was with the Laboratory of Radiocommunication where he worked on antennas coupling in the VHF-HF band. He received the Ph.D. degree in 1999 from the SEI (Système Électronique et Informatique) Laboratory. Now, he is with IETR Laboratory (Institut d'Électronique et de Télécommunications de Rennes) at Polytech'Nantes (University of Nantes, France). He works as a Researcher of National Center for Scientific Research on electromagnetic wave scattering from rough surfaces and objects for remote sensing applications. He is author of more than 90 journal articles and conference papers.

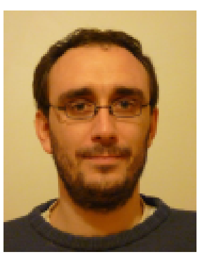

Nicolas Pinel was born in Saint-Brieuc, France, in 1980. He received the Engineering degree and M.S. degree in Electronics and Electrical Engineering both from Polytech Nantes (Ecole polytechnique de l'université de Nantes), Nantes, France, in 2003. He received the Ph.D. degree from the University of Nantes, France, in 2006. He is currently working as a research Engineer in IETR Laboratory (Institut d'Électronique et de Télécommunications de Rennes), Nantes, France, and is going to join Alyotech Technologies, Rennes, France. His research interests are in the areas of radar and optical remote sensing, scattering and propagation. In particular, he works on asymptotic methods of electromagnetic wave scattering from random rough surfaces and layers.

Janic Chauveau was born in Saint-Nazaire, France, in 1981. He received the M.S. degree in electronics and electrical engineering from Polytech'Nantes Ecole polytechnique de l'universit de Nantes), Nantes, France, in 2004. He received the Ph.D. degree from the University of Nantes, France, in 2007. He is currently working in the field of radar signatures at the Direction Générale de l'Armement (DGA), DGA-Maîtrise de l'Information, Bruz, France. His research interests include electromagnetic scattering and inverse scattering problems.